J|A|C|S ARTICLES

Published on Web 09/10/2009

Facile Photochemical Synthesis and Characterization of Highly Fluorescent Silver Nanoparticles

Luca Maretti, Paul S. Billone, Yun Liu, and Juan C. Scaiano*

Centre for Catalysis Research and Innovation and Department of Chemistry, University of Ottawa, 10 Marie Curie, Ottawa K1N 6N5, Canada

Received January 10, 2009; E-mail: tito@photo.chem.uottawa.ca

Abstract: Highly fluorescent silver nanoparticles (AgFNP) have been prepared by a facile photochemical method, yielding these materials in just a few minutes and with excellent long-term stability. The method makes use of photogenerated ketyl radicals that reduce Ag^+ from silver trifluoroacetate in the presence of amines. While as functional materials these AgFNP can be described as of nanometer dimensions, we believe that the luminescence arises from particle-supported small metal clusters (predominantly Ag_2). The materials have been characterized by electron microscopy, fluorescence and absorption spectroscopy, fluorescence lifetime studies, and ^{19}F NMR spectroscopy. Exploratory work shows that the fluorescence from AgFNP can be efficiently quenched by paramagnetic quenchers, and these studies have been combined with electron paramagnetic resonance work.

Introduction

Research on fluorescent nanoparticles concentrates mainly on semiconductor particles, usually referred to as quantum dots.[1] Among these, CdSe particles, either core-only or core−shell, are the most widely studied. In the case of CdSe core−shell quantum dots, the shell (frequently ZnS)[2] makes the particles more strongly fluorescent and significantly more robust. The fluorescence of CdSe quantum dots can be readily tuned across the visible spectrum. In spite of their widespread use, quantum dots frequently present problems related to the intrinsic blinking of their luminescence, and to toxicity issues that limit their applications in the health sciences.[3] Further, while a shell makes them more robust, it also limits their use in some sensing applications, since the same shell that brings these benefits also reduces their sensitivity to potential solution analytes.[4,5]

Metal nanoparticles, particularly those from coin metals, are expected to have lower toxicity and can be readily prepared reproducibly and with excellent solution stability. Particles of a few nanometers in diameter frequently display a plasmon absorption that in the case of gold and silver is readily detectable in the visible spectral region.[6−8] This absorbance is due to the collective oscillation of the electrons in the conduction band and is not associated with any significant emission, although other chromophores near the surface can undergo enhanced transitions, sometimes resulting in increased luminescence.[9,10]

In contrast with metal nanoparticles in the nanometer scale, very small clusters can show remarkably strong emission.[11−29] In the case of silver, clusters such as Ag_2, Ag_3, and Ag_4 have

(1) Alivisatos, A. P. *Science* **1996**, *271*, 933–937.
(2) Dabboussi, B. O.; Rodriguez-Viejo, J.; Mikulec, F. V.; Heine, J. R.; Mattoussi, H.; Ober, R.; Jensen, K. F.; Bawendi, M. G. *J. Phys. Chem. B* **1997**, *101*, 9463–9475.
(3) Medintz, I.; Mattoussi, H.; Clapp, A. *Int. J. Nanomed.* **2008**, *3*, 151–167.
(4) Heafey, E.; Laferrière, M.; Scaiano, J. C. *Photochem. Photobiol. Sci.* **2007**, *6*, 580–584.
(5) Rene-Boisneuf, L.; Scaiano, J. C. *Chem. Mater.* **2008**, *20*, 6638–6642.
(6) Burda, C.; Chen, X.; Narayanan, R.; El-Sayed, M. A. *Chem. Rev.* **2005**, *105*, 1025–1102.
(7) Henglein, A. *Chem. Rev.* **1989**, *89*, 1861–1873.
(8) Kamat, V. K. *J. Phys. Chem. B* **2002**, *106*, 7729–7744.
(9) Lakowicz, J. R. *Anal. Biochem.* **2005**, *337*, 171–194.
(10) Tam, F.; Goodrich, G. P.; Johnson, B. R.; Halas, N. J. *Nano Lett.* **2007**, *7*, 496–501.
(11) Zheng, J.; Nicovich, P. R.; Dickson, R. M. *Annu. Rev. Phys. Chem.* **2007**, *58*, 409–431.
(12) Zheng, J. P. J. T.; Dickson, R. M. *J. Am. Chem. Soc.* **2003**, *125*, 7780–7781.
(13) Vosch, T.; Antoku, Y.; Hsiang, J.-C.; Richards, C. I.; Gonzalez, J. I.; Dickson, R. M. *Proc. Natl. Acad. Sci. U.S.A.* **2007**, *104*, 12616–12621.
(14) Petty, J. T.; Zheng, J.; Hud, N. V.; Dickson, R. M. *J. Am. Chem. Soc.* **2004**, *126*, 5207–5212.
(15) Yu, J.; Patel, S. A.; Dickson, R. M. *Angew. Chem., Int. Ed.* **2007**, *46*, 2028–2030.
(16) Zheng, J.; Dickson, R. M. *J. Am. Chem. Soc.* **2002**, *124*, 13982–13983.
(17) Rabin, I.; Schulze, W.; Ertl, G. *J. Chem. Phys.* **1998**, *108*, 5137–5142.
(18) Zhang, J.; Xu, S.; Kumacheva, E. *Adv. Mater.* **2005**, *17*, 2336–2340.
(19) Alqudami, A.; Annapoorni, S. *Plasmonics* **2007**, *2*, 5–13.
(20) Shen, Z.; Duan, H.; Frey, H. *Adv. Mater.* **2007**, *19*, 349–352.
(21) Shang, L.; Dong, S. *Chem. Commun.* **2008**, 1088–1090.
(22) Rabin, I.; Schulze, W.; Ertl, G. *Chem. Phys. Lett.* **1999**, *312*, 394–398.
(23) Rabin, I.; Schulze, W.; Ertl, G.; Felix, C.; Sieber, C.; Harbich, W.; Buttet, J. *Chem. Phys. Lett.* **2000**, *320*, 59–64.
(24) Felix, C.; Sieber, C.; Harbich, W.; Buttet, J.; Rabin, I.; Schulze, W.; Ertl, G. *Phys. Rev. Lett.* **2001**, *86*, 2992–2995.
(25) Fedrigo, S.; Harbich, W.; Buttet, J. *J. Chem. Phys.* **1993**, *99*, 5712–5717.
(26) Treguer, M.; Rocco, F.; Lelong, G.; Le Nestour, A.; Cardinal, T.; Maali, A.; Lounis, B. *Solid State Sci.* **2005**, *7*, 812–818.
(27) Makarava, N.; Parfenov, A.; Baskakov, I. V. *Biophys. J.* **2005**, *89*, 572–580.
(28) Maali, A.; Cardinal, T.; Treguer-Delapierre, M. *Physica E* **2003**, *17*, 559–560.
(29) Sengupta, B.; Ritchie, C. M.; Buckman, J. G.; Johnsen, K. R.; Goodwin, P. M.; Petty, J. T. *J. Phys. Chem. C* **2008**, *112*, 18776–18782.

10.1021/ja900201k CCC: $40.75

well characterized fluorescence.[17,23,25,30] This emission has molecular-type properties, relatively long lifetimes and a good mirror-image relationship between absorption and emission. However, these aggregates by themselves are effectively too small and unstable for many practical applications, and it is desirable to stabilize or encapsulate them with other materials to make them suitable for applications in sensing, chemical biology, or advanced materials.[13]

The vast majority of reductive processes leading to metal nanoparticles rely on the use of thermal methods, such as citrate or borohydride reduction.[31,32] Some applications make use of photochemical methods that offer temporal and spatial control (as needed for imaging applications) and where the rate of reduction can be readily controlled by adjusting the incident light intensity.[33,34] Remarkably, most reports concerned with photoinitiated synthesis of metal nanoparticles do not give particular consideration to the absorption properties of the substrate, the detailed emission properties of the light source, or the possibilities that quenching mechanisms will vastly reduce the efficiency with which the synthesis takes place. In recent publications we have addressed some of these issues in relation to the photochemical synthesis of silver and gold nanoparticles.[33−35]

In this contribution we report a new method for the facile photochemical synthesis of highly fluorescent functional silver nanoparticles. These particles are very stable and can be reliably and reproducibly synthesized. While the observable silver fluorescent nanoparticles (AgFNP) are of nanometer dimensions, we believe that the emission arises from nanoparticle-supported small metal clusters, a conclusion based on their spectroscopic properties, and the fact that no "plasmon emission" should be anticipated. Luminescence from small clusters on particle surfaces is rare but not unprecedented.[26]

Experimental Section

Unless otherwise indicated, solvents and reagents were purchased from Aldrich and used as received. Irgacure-2959 (I-2959) (1-[4-(2-hydroxyethoxy)phenyl]-2-hydroxy-2-methyl-1-propan-1-one) was a generous gift from Ciba Specialty Chemicals. I-2959 is an efficient source of ketyl radicals.[35,36]

The size of the nanoparticles was determined by transmission electron microscopy (TEM), while the crystalline structures of the nanoparticles were characterized by high-resolution transmission electron microscope (HRTEM). Both TEM and HRTEM studies were performed using a JEOL JEM-2100F field emission transmission electron microscope equipped with an ultra high resolution pole-piece operating at 200 kV. An Oxford energy dispersive X-ray spectrometer (EDS) attached to the JEM-2100F microscope was used to determine the elemental composition of the nanoparticles. TEM specimens were prepared by placing microdrops of nanoparticle solution directly onto a copper grid coated with carbon film (300 mesh, EMS).

All the steady-state emission spectra were recorded using a Photon Technology International spectrofluorimeter. Lifetime fluorescence measurements were performed on an Easylife LS (Photon Technology International). The excitation was performed with a 440 nm pulsed LED, and the broadband emission was measured using a 10 nm bandpass filter centered at 540 nm.

All absorption spectra were recorded on a Varian CARY-50 UV−vis spectrophotometer. All samples were placed in UV quality quartz cuvettes, 1 cm path length unless otherwise noted. The resolution of our measurements was set to 1 nm. Some experiments required the use of cuvettes with a 3 mm path length, since otherwise the absorbance exceeded 3.0 and was beyond the reliable dynamic range of the spectrometer.

The samples were exposed to ultraviolet light in a Luzchem photoreactor equipped with UVA lamps. Typically the unit was operated with four lamps, corresponding to about 26 W/m^2 with approximately 4% spectral contamination, mostly visible and UVB light.

^{19}F were performed on a Bruker AVANCE 300 NMR spectrometer. The solvent used in all cases was toluene-d_8. ^{19}F spectra were recorded using a 2.59 s acquisition time with 0.3 Hz of line broadening, proton decoupling, and 12626 Hz spectral width. An external chemical shift standard of 0.05% trifluorotoluene (−63.72 ppm) was used to calibrate ^{19}F chemical shift values.

EPR measurements were performed using a JEOL FA-100 X-Band EPR spectrometer equipped with a JEOL ES-UCX2 cylindrical cavity. Samples were deaerated with nitrogen prior to measurements and held in clear-fused silica tubes (5 mm diameter) purchased from Wilmad. All spectra were recorded over 2 min at 0.1 mW power, modulation width of 0.01 mT, time constant of 0.03 s, and a sweep width of 5 mT.

Fluorescence microscopy studies employed a Leica DMLS optical microscope, with a 50 W mercury lamp which provided the excitation lamp, and a Leica DFC 300 FX camera. Solutions were spin-coated on 1 inch diameter fused silica discs at 2000 rpm for 20 s, using a spin-coater from Specialty Coatings, Inc. The solution was prepared by dissolving 200 mg of polystyrene in 5 mL of toluene and then adding appropriate amounts of silver trifluoroacetate, I-2959, and hexadecylamine. Solutions were used on the same day in which they were prepared. Films were exposed to UVA light at approximately 13 W m^{-2}.

Results

Photochemical Synthesis and UV−Visible Spectroscopy. Experiments were performed in toluene and in tetrahydrofuran (THF), mostly under nitrogen and occasionally under air. The samples were deaerated by bubbling with nitrogen for at least 30 min. Both solvents of choice are transparent in the UVA region used for exposure during the AgFNP synthesis.

Ketyl radicals are known to be strong reducing agents, suitable for metal ion reduction.[35,37−39] In our case we chose I-2959 as our source of ketyl radicals; the choice reflects the excellent absorption properties of I-2959 in the UVA region, the high quantum yield of radical generation, and the fact that the short triplet lifetime of I-2959 reduces the likelihood of excited state quenching by other solution components,[36] notably amines[40] and silver ions.[33] Scheme 1 shows the proposed mechanism for the formation of silver nanoparticles.

The spectral changes observed upon irradiation (4 UVA lamps) of a quartz cuvette containing 2 mM each of $AgCF_3COO$, I-2959, and cyclohexylamine are shown in Figure 1. Approximately 80% of the maximum achievable absorption is

(30) Felix, C.; Sieber, C.; Harbich, W.; Buttet, J.; Rabin, I.; Schulze, W.; Ertl, G. *Chem. Phys. Lett.* **1999**, *313*, 105–109.
(31) Turkevich, J.; Stevenson, P. C.; Hiller, J. *Discuss. Faraday Soc.* **1951**, *11*, 55–75.
(32) Brust, M.; Walker, M.; Bethell, D.; Schiffrin, D. J.; Whyman, R. *J. Chem. Soc., Chem. Commun.* **1994**, 801–802.
(33) Scaiano, J. C.; Aliaga, C.; Maguire, S.; Wang, D. *J. Phys. Chem. B* **2006**, *110*, 12856–12859.
(34) McGilvray, K. L.; Decan, M. R.; Wang, D.; Scaiano, J. C. *J. Am. Chem. Soc.* **2006**, *128*, 15980–15981.
(35) Marin, M. L.; McGilvray, K. L.; Scaiano, J. C. *J. Am. Chem. Soc.* **2008**, *130*, 16572–16584.
(36) Jockusch, S.; Landis, M. S.; Freiermuth, B.; Turro, N. J. *Macromolecules* **2001**, *34*, 1619–1626.
(37) Hada, H.; Yonezawa, Y.; Akio, Y.; Kurakake, A. *J. Phys. Chem.* **1976**, *80*, 2728–2731.
(38) Kometani, N. D. H.; Asami, K.; Yonezawa, Y. *PCCP* **2002**, *4*, 5142–5247.
(39) Henglein, A.; Tausch-Treml, R. *J. Colloid Interface Sci.* **1981**, *80*, 84–93.
(40) Cohen, S. G.; Parola, A.; Parsons, G. *Chem. Rev.* **1973**, *73*, 141–161.

Scheme 1. Mechanism for the Formation of Stabilized AgFNP

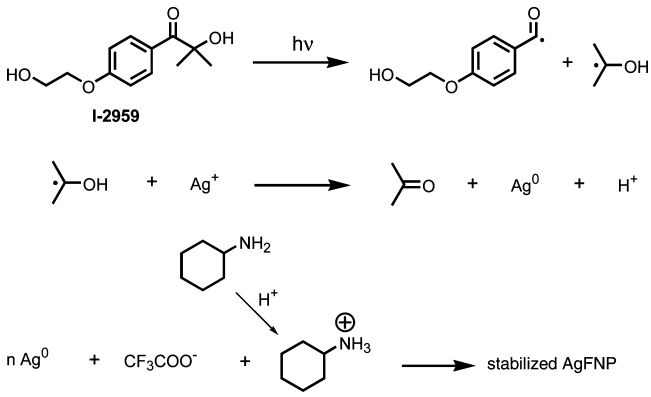

reached within 3 min of exposure. The maximum is initially at 447 nm and gradually shifts to 449 nm; it is likely that this shift simply reflects an underlying increase in light scattering or the formation of plasmon absorbance due to nanoparticles (vide infra). The particles produced in this manner were stable for at least several months, even in the presence of air and without protection from ambient light.

While cyclohexylamine proved to be effective in the formation and stabilization of these particles, other amines were also found to work. While our search was not exhaustive, for example, hexadecylamine also gave excellent results. Many other amines, including triethylamine and butylamine, were tested and did not yield fluorescent particles, resulting sometimes in cloudy orange/brown suspension, suggestive of extensive nanoparticle aggregation. Absorbance spectra of samples prepared with triethylamine and in the absence of amine are presented in the Supporting Information (Figure S3). With triethylamine, a week absorption band is visible at 415−420 nm, with no associated fluorescence, and there is significant optical scattering at longer irradiation times, indicative of the formation of large aggregates of Ag nanoparticles or bulk silver.

The growth plot for hexadecylamine also shows a maximum at 449 nm and is slightly lower than that for cyclohexylamine. The two growth plots are compared in Figure 2. Interestingly, with hexadecylamine at irradiation times longer than 300 s we observe a small band at 552 nm, possibly due to larger aggregates (vide infra).

While toluene proved an excellent solvent for AgFNP synthesis, a few other solvents were tested. Among these, THF proved to be a convenient one.

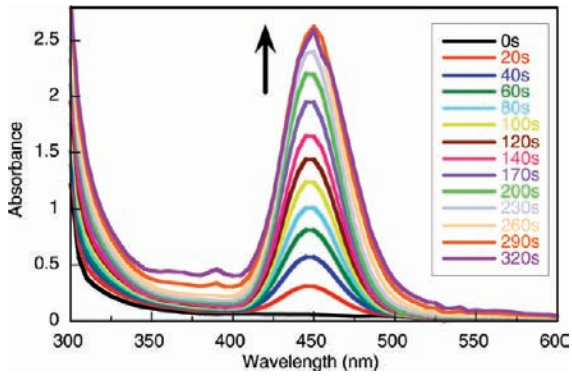

Figure 1. UV/vis absorption spectra following irradiation (350 nm, four lamps) of a toluene solution containing 2 mM silver trifluoroacetate, 2 mM I-2959, 2 mM cyclohexylamine. Reaction performed and monitored directly in a 0.7 × 0.3 cm quartz cuvette.

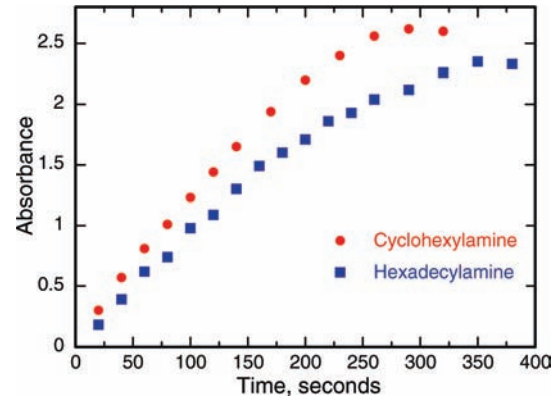

Figure 2. Growth of the 450 nm absorption band upon irradiation (350 nm, four lamps) in toluene. Initial concentrations: 2 mM silver trifluoroacetate, 2 mM I-2959, 2 mM amine. Reaction performed in 0.7 × 0.3 cm quartz cuvette.

In a typical experiment, a nitrogen-saturated THF solution of 5.0 mM $AgCF_3COO$, 5.0 mM cyclohexylamine, and 5.0 mM I-2959 was irradiated with UVA light. Upon irradiation, we observe the growth of a sharp absorption band centered at 438 nm with a smaller peak at 390 nm (Figures 1 and below in Figure 5). Control reactions were performed in the absence of the photoinitiator at the same working concentrations, and no absorption was observed. The concentration of starting reagents was also varied from 2 to 30 mM for each component. When the concentrations were kept equimolar and below 10 mM, an absorption band centered at 438 nm was observed to grow upon photolysis in THF as solvent. The most significant difference between these experiments was that the value at which the absorption band was found to plateau increased with increasing concentrations. However, the decay of the absorption band (vide infra) was also accelerated at higher concentrations; thus, 5 mM was adopted as the optimal compromise between signal intensity and stability. The spectra of reaction mixtures performed at various concentrations are included in the Supporting Information (Figure S2). At higher concentrations (30 mM of each), a thermal reaction occurred over several hours and similar absorption and emission peaks were observed. This thermal reaction was extremely sensitive to the age and quality of both reagents and solvent and was of limited use because of its irreproducibility. The use of amines as reducing agents had previously been reported as a route to metallic nanoparticles.[41]

The effect of oxygen on the synthesis of AgFNP was also examined in THF. The only significant effect observed in aerated solutions was an approximately 2 min induction period, which we attribute to the sacrificial use of some of the initially photogenerated radicals to consume the dissolved oxygen; we note that since the samples are not stirred and the irradiation times quite short, oxygen is unlikely to be significantly replenished from the gas phase. Interestingly, the reaction of ketyl radicals with oxygen yields superoxide radicals (or HO_2• in nonpolar solvents).[42,43] It would seem that under our experimental conditions, HO_2• does not reduce Ag^+ to Ag^0. The maximum under these conditions was at about 438 nm, slightly blue-shifted with respect to that observed in toluene.

(41) Newman, J. D. S. B. G. J. *Langmuir* **2006**, *22*, 5882–5887.
(42) Maillard, B.; Ingold, K. U.; Scaiano, J. C. *J. Am. Chem. Soc.* **1983**, *105*, 5095–5099.
(43) Ingold, K. U.; Paul, T.; Young, M. J.; Doiron, L. *J. Am. Chem. Soc.* **1997**, *119*, 12364–12365.

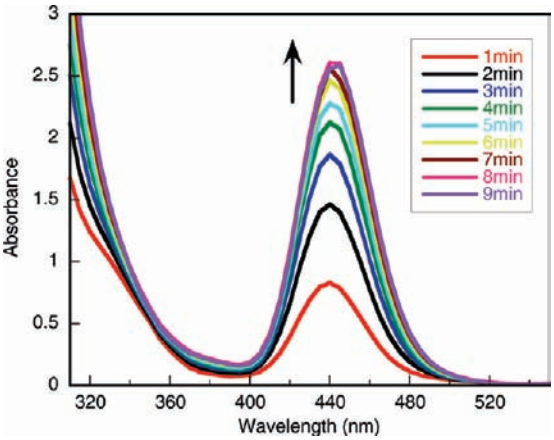

Figure 3. UV/vis absorption spectra at various time intervals during irradiation (350 nm, four lamps) directly in THF. Initial concentrations: 5 mM silver trifluoroacetate, 5 mM I-2959, 5 mM cyclohexylamine. Reaction performed in 1 × 1 cm quartz cell.

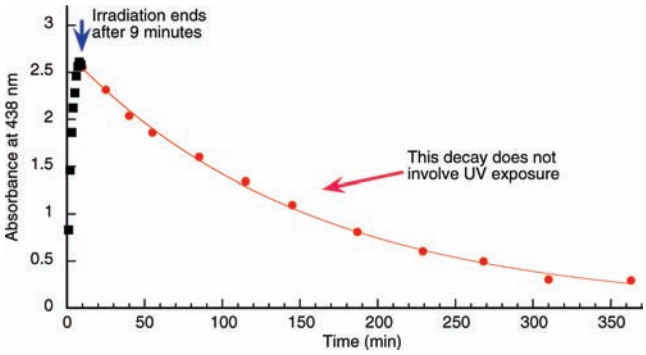

Figure 4. Growth and decay of the absorbance at 438 nm following 9 min. UVA exposure under the same conditions as in Figure 3.

In contrast to the case of toluene where particles are stable for months, this is not the case in THF, where particles decay over a few hours, as shown in Figure 4. The thermal decay of the absorbance in THF follows a clean monoexponential decay with a lifetime of 154 min.

We believe that the instability in THF is due to dissolution of the ammonium trifluoroacetate salt which forms a major part of the stabilizing layer on the particles, as indicated by NMR results (vide infra). Given the lack of long-term stability shown in Figure 4, one could assume that synthesis in THF solvent was simply not practical. However, imaging data (vide infra) suggests that use of THF for nanoparticle synthesis leads to narrower polydispersity than in the case of toluene. This led us to explore ways of purifying particles originally made in THF to enhance their long-term stability. Transfer to toluene was an obvious choice, given the recorded stability in this solvent. After THF evaporation we added toluene to yield a bright yellow solution and a white precipitate which was filtered and characterized as 4-ethanoloxybenzoic acid (an oxidation product of the benzoyl radical of Scheme 1). We found that upon redispersion in toluene, the particles were stable for several weeks when stored at −5 °C. Upon standing at −5 °C, a white precipitate is formed and characterized as excess cyclohexylammonium salt **2** present in the reaction mixture. Sometimes after removal of the sample from the fridge and re-equilibration to room temperature the particles decomposed quickly giving a brown solution. We believe the stability following removal to room temperature is an indication of how much salt **2** had

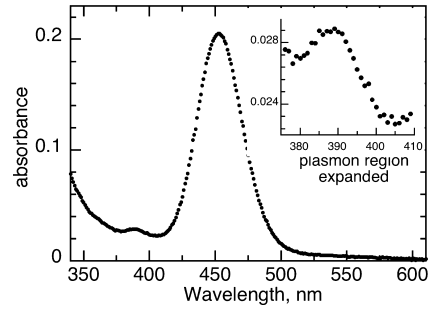

Figure 5. UV/vis absorption spectrum of Ag particles in toluene prepared using the same procedure as in Figure 3 followed by transfer to toluene. The inset shows the band we believe to be due to the residual plasmon absorption.

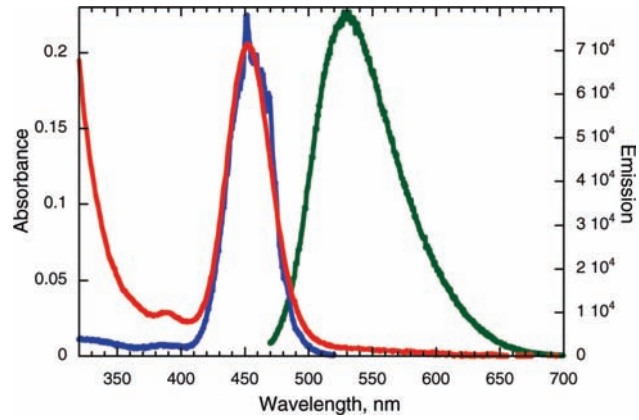

Figure 6. Absorption (red), emission (green), and excitation (blue) spectra of Ag particles after 4 min of irradiation in THF under the conditions of Figure 3 and resuspension in toluene.

precipitated from solution; when too much **2** was precipitated due to extended storage at −5 °C, the particles decomposed quickly upon warming to room temperature. In addition we observed shifts in the absorption and emission bands to ∼450 and 530 nm, respectively (vide infra). This change may be due to the difference in dielectric constants of the two solvents[44] as well as to the degree of surface coverage by the quaternary ammonium salt.

It was interesting to note that in addition to the strong absorption band (at 452 nm after toluene resuspension), we also observed a weak but characteristic peak at approximately 390 nm, as shown in the inset in Figure 5. As we will argue in the Discussion, we do not believe that the bands around 450 nm are due to the plasmon band, but it is likely that the absorbance at 390 nm (with no associated emission) is due to plasmon transitions.

Fluorescence Spectroscopy. The nanoparticles described in the preceding section showed strong luminescence in the visible region. Figure 6 shows the emission, excitation, and absorbance spectra from a sample irradiated for 4 min under the conditions described above.

Detailed emission and excitation spectra are included in the Supporting Information. Interestingly, in THF the emission was quite red-shifted (λ_{max} 580 nm) with respect to the maximum at 528 nm observed in toluene. The sample yielding the fluorescence spectra in THF solution contains not only silver nanoparticles but also the photoproducts originating from the

(44) Link, S.; El-Sayed, M. A. *J. Phys. Chem. B* **1999**, *103*, 8410–8426.

Table 1. Fluorescence Quantum Yields in Toluene for Various AgFNP Determined Using Fluorescein as a Reference Standard and for Different Synthesis Solvents

solvent	synthesis amine	Φ_{F1}[a] (±10%)
toluene	hexadecylamine	0.11
toluene	cyclohexylamine	0.15
THF	cyclohexylamine	0.11

[a] Fluorescein standard. Excitation wavelength 450 nm.

photodecomposition of I-2959 (these products emit weakly at 465 nm). Instead, the fluorescence spectra obtained in toluene solutions of samples originally prepared in THF reflect AgFNP that have been purified by the cooling/filtration process.

The determination of quantum yields was carried out using fluorescein as an emission standard. It is important to select a reference compound with an adequate spectral overlap with the material under study.[5] Relevant spectra are shown in the Supporting Information. We note that all too frequently Rhodamine 6G is used as a reference, even when it has little or no overlap with the emission of the sample under study.[5] Equation 1 shows the expression used for the case of toluene and includes an appropriate refractive index correction.

$$\Phi_{\text{sample}} = \Phi_{\text{ref}} \times \frac{I_{\text{sample}}}{I_{\text{ref}}} \times \frac{A_{\text{ref}}}{A_{\text{sample}}} \times \frac{\eta^2_{\text{sample}}}{\eta^2_{\text{ref}}} \qquad (1)$$

where Φ_{ref} is the known quantum yield of the reference compound, I_{sample} and I_{ref} are the integrated fluorescence intensities of the sample and reference, respectively, A_{ref} and A_{sample} are the absorbance of the reference and the sample at the excitation wavelength, and η_{sample} and η_{ref} are the refractive index of the sample solvent and reference solvent, respectively.

The fluorescence quantum yields obtained are summarized in Table 1 and are based on the integrated fluorescence between 470 and 700 nm. The absorbance of each sample and the fluorescein reference at 450 nm (excitation wavelength) was 0.090 (Figure S4).

The fluorescence quantum yields obtained are quite high, making their emission readily observable under weak irradiation conditions, such as those available from laboratory TLC lamps. An example of the observed emission is presented in the Table of Contents graphic for this contribution.

Fluorescence Lifetimes. In our laboratory we are used to examining fluorescence decay behavior in quantum dots, where complex decays requiring lifetime distribution analysis are the rule. We were thus surprised to discover that in the case of AgFNP the decays (>98%) could be readily fitted with a monoexponential expression. In the case of toluene the decay was fit to a monoexponential function with a lifetime of 2.6 ± 0.1 ns and a goodness of fit $\chi^2 = 1.46$. The corresponding decay and instrument functions are shown in Figure 7. Similar lifetimes have been recorded in DNA encapsulated systems,[13] while in argon matrixes the lifetime of Ag_2 clusters has been reported as 4.6 ns.[45]

NMR Spectroscopy. Our synthesis experiments showed unequivocally that the presence of trifluoroacetate anions was critical for the preparation of highly fluorescent AgFNP. That is, while the reduction of Ag^+ by I-2959 would occur regardless of the presence of this anion, the particles would not normally fluoresce. For example, silver nitrate is readily reduced in the

(45) Konig, L.; Rabin, I.; Schulze, W.; Ertl, G. *Science* **1996**, *274*, 1353–1355.

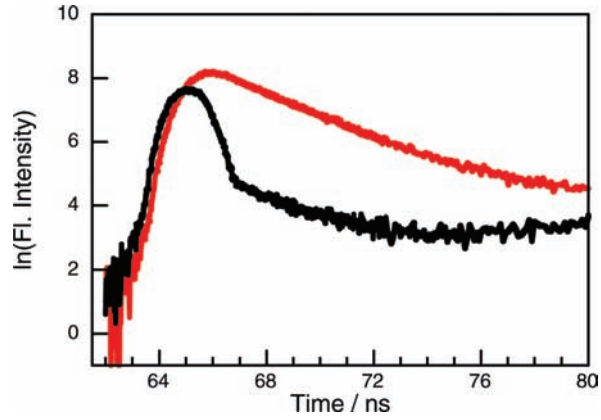

Figure 7. Fluorescence lifetime of Ag particles in toluene, as prepared in Figure 1 and diluted to an appropriate concentration, with excitation at 440 nm and detection at 550 nm (red). The instrument response function (black) is also included.

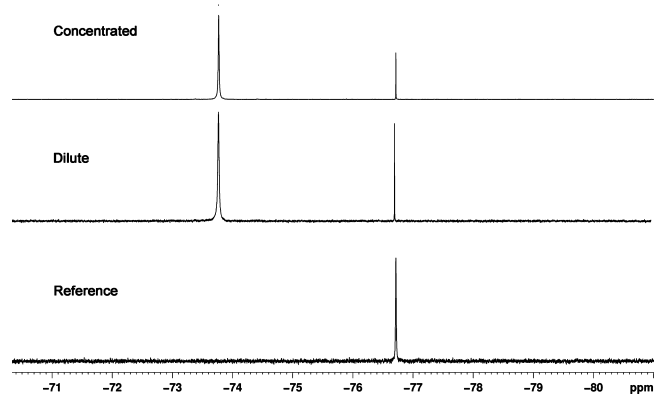

Figure 8. ^{19}F NMR spectra of concentrated (A) and dilute (B) hexadecylamine−Ag particles following the cooling/filtration procedure described in the text. Spectrum C is the independently prepared hexadecylammonium trifluoroacetate salt. All samples were prepared in toluene-d_8, and additional details are included in the Experimental Section.

presence of photochemically generated ketyl radicals but the product is not fluorescent. ^{19}F NMR is a sensitive technique offering excellent diagnostics for the environment of ^{19}F atoms.

The ^{19}F NMR data for AgFNP prepared in toluene with hexadecylamine are shown in Figure 8. Spectrum C shows a reference spectrum from hexadecylammonium trifluoroacetate. Spectrum A clearly shows that the ^{19}F peak is considerably shifted to −73.76 ppm (compared to −76.71 ppm for the reference). As the sample is diluted (spectrum B), the relative importance of the reference peak also increases. In both spectrum A and spectrum B, a significant broadening of the peak centered at −73.76 is observed.

A number of important conclusions can be drawn from the NMR spectra of Figure 8. First, the trifluoroacetate anion is in a different environment when the AgFNP are present, as would be expected if they form part of a nanoparticle stabilizing layer. Second, the increased peak width is consistent with restricted mobility and an exchange time similar to or longer than the time scale of the NMR response. Third, the fact that the proportion of free anion increases upon dilution is a clear indication of a dynamic equilibrium between associated and free ions. Our experiments do not show if all, or only part, of the stabilizing anions are exchangeable.

NMR experiments were also performed when the stabilizing salt was based on cyclohexylamine; the corresponding spec-

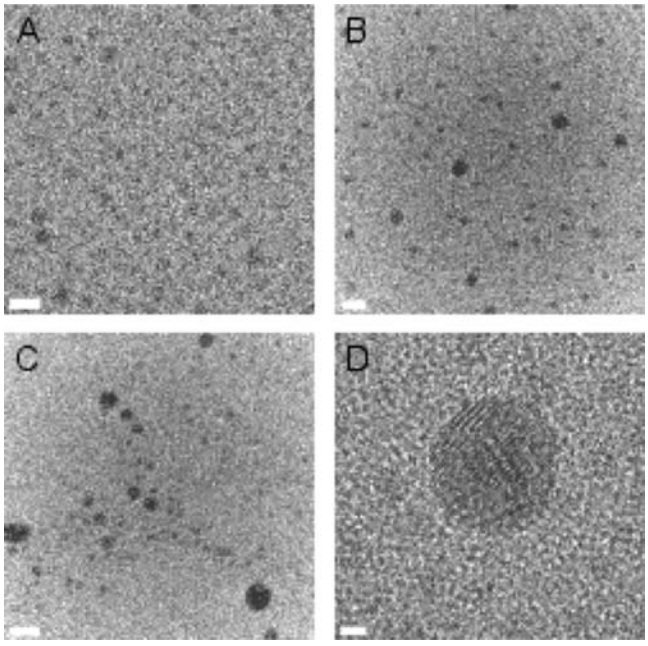

Figure 9. TEM images of AgFNPs prepared using different procedures: (A) particles synthesized in THF with cyclohexylamine, redispersed in toluene, and dropcast from toluene; (B) particles synthesized in toluene with cyclohexylamine, purified as discussed in the text, and dropcast from toluene; (C) particles synthesized in toluene with hexadecylamine, purified as discussed in the text, and dropcast from toluene; (D) HR-TEM image of a large particle in sample a. Scale bars are 10, 20, 20, and 2 nm for A, B, C, and D, respectively.

troscopic data are included in the Supporting Information. Briefly, similar trends are observed in all systems examined, but for cyclohexylamine the ^{19}F peak is broader and shows some shifts with concentration, suggesting that more than one site may be available to the trifluoroacetate anion. The fact that the behavior depends on the counterion (i.e., the protonated amine) suggests that the ammonium ion must also be part of the stabilizing layer, as suggested in Scheme 1.

Attempts to monitor ^{1}H NMR for the amine were inconclusive, although it is clear that the presence of AgFNP influenced the spectrum, also consistent with the amine forming part of the particle-stabilizing layer (Figure S6b). There are literature reports indicating that base sites may contribute to AgFNP stabilization.[29]

Nanoparticle TEM Imaging. TEM imaging experiments were performed on samples dispersed in toluene, using both solutions obtained directly in this solvent, as well as particles originally made in THF and then resuspended in toluene, as described in the AgFNP synthesis section. This purification procedure was found to minimize the presence of organic crystals in the image.

Measurement of a range of particles prepared in THF leads to an average size of (3.4 ± 0.7) nm for AgFNP obtained by the same protocol as in Figure 9 (see histogram in Supporting Information).

Analysis of the crystal lattice spacing clearly shows Ag(1,1,1) with its characteristic 0.236 nm spacing (Figure 9d). We note that while some single crystal particles are detected, the majority proved polycrystalline. EDS characterization of the particles showed that they are composed of metallic silver, as expected. XPS measurements were attempted on the same samples used for TEM microscopy but only confirmed the presence of Ag^0 and Ag^{1+}, the latter likely from residual unreacted silver trifluoroacetate.

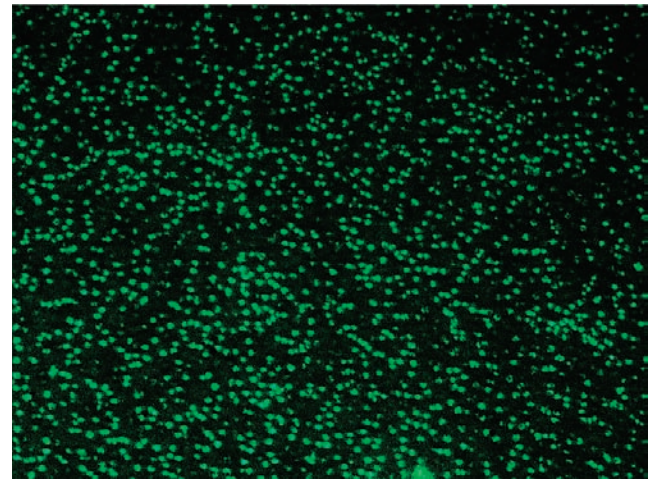

Figure 10. Fluorescence microscopy image (100×) of a polystyrene (PS) film containing hexadecylamine−AgFNP with (microscope) excitation at 436 nm and broadband detection at $\lambda > 470$ nm. The sample was prepared by UVA photolysis of a spin-coated PS film containing 20 mM silver trifluoroacetate, 20 mM I-2959, and hexadecylamine for 20 min. Spot size is diffraction-limited (>300 nm) and shows correctly particle location but not dimensions.

Fluorescence Microscopy in Polymer Films. While this study is at present at a very preliminary stage and its lithographic applications will be the subject of a future report, fluorescence microscopy images in polystyrene films (as close as possible to the toluene solvent used here) were used to explore the nature of the fluorescent material studied here. For this purpose, solutions of similar composition as those described above, but containing polystyrene, were spin-coated on fused silica disks and exposed to UVA light. Figure 10 shows an image obtained in this manner.

Figure 10 demonstrates unequivocally that the emission arises from discrete particles and thus Ag emissive clusters must be located at or near the AgNP surface. The fact that small (predominantly Ag_2) fluorescent clusters are associated with larger nanoparticles is also consistent with the fluorescence quenching studies reported in the next section. While our data are consistent with the absorption, emission spectra, and fluorescence lifetime for Ag_2, we cannot rule out possible involvement of species such as Ag_3 and Ag_4. A fluorescence spectrum of a single fluorescing particle from Figure 10 has been included in the Supporting Information.

Fluorescence Quenching Studies. Our recent studies of CdSe quantum dots[4,46−48] have led us to the conclusion that nitroxides are excellent quenchers of nanoparticle fluorescence and that these studies can yield information on the form of quenching, the nature of binding interactions, the ligand environment at the nanoparticle surface, and the dynamics of quencher−surface interactions. Among the nitroxides tested, 4-amino-TEMPO, 4aT, proved very convenient, with excellent surface binding properties.[4,47] Amines are known to bind well to noble metal particles.[8]

Stern−Volmer analysis is a common technique used to acquire information regarding fluorescence quenching mech-

(46) Laferriere, M.; Galian, R. E.; Maurel, V.; Scaiano, J. C. *Chem. Commun.* **2006**, 257–259.
(47) Maurel, V.; Laferriere, M.; Billone, P.; Godin, R.; Scaiano, J. C. *J. Phys. Chem. B* **2006**, *110*, 16353–16358.
(48) Scaiano, J. C.; Laferriere, M.; Galian, R. E.; Maurel, V.; Billone, P. *Phys. Status Solidi A* **2006**, *203*, 1337–1343.

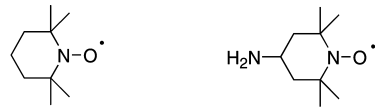

TEMPO 4aT

anisms[49,50] and has proven useful in the interpretation of the quenching experiments with CdSe quantum dots.[47,48,51,52] Briefly, when the mechanism for deactivation of an excited state, fluorescent in the present case, is a simple competition between first-order processes that determine the excited state lifetime, τ (fluorescence, intersystem crossing, thermal deactivation), and a bimolecular quenching process by some quencher Q with rate constant k_q, the fluorescence intensity in the absence of quencher, F_0, and in the presence of quencher, F, can be related by eq 2, where $k_q\tau = K_{SV}$.[50]

$$\frac{F_0}{F} = 1 + k_q\tau[Q] = 1 + K_{SV}[Q] \qquad (2)$$

Quenching experiments were performed in toluene with AgFNP prepared directly in this solvent. The corresponding Stern−Volmer quenching plot is shown in Figure 11 and also includes a 4aT quenching plot recorded in the presence of 40 μM cyclohexylamine. The fact that cyclohexylamine attenuates the quenching by 4aT is a clear indication that the amine groups in 4aT and cyclohexylamine compete for binding sites at the AgFNP surface. The data has been fit with a parabola for convenience; the linear coefficient of the fit corresponds to the initial slope (i.e., lim[4aT] → 0), yielding values of 44 200 M^{-1} and 30 100 M^{-1} in the absence and presence of 40 μM cyclohexylamine, respectively.

It is important to note that both primary amine and free radical functionalities are essential for quenching where the amine group provides only a binding interaction, as cyclohexylamine addition by itself has almost no effect on fluorescence. On the other hand, TEMPO itself is a poor quencher, and 15 mM TEMPO leads to a quenching ratio F_0/F of 2.6; the same value can be achieved with ~30 μM 4aT (see Figure 11). Thus, 4aT is approximately 400 times more efficient than TEMPO as a quencher. Quenching data for TEMPO have been included in the Supporting Information.

Given $K_{sv} = k_q\tau$, where k_q is the bimolecular rate constant for excited state quenching and τ the excited state lifetime, then it is possible to extract k_q, given the knowledge of τ from fluorescence studies ($\tau \sim 2.6$ ns in toluene). This analysis yields a value of $k_q = 1.7 \times 10^{13}$ M^{-1} s^{-1} (from the initial slope in Figure 11). This number is 3 orders of magnitude larger than that for a diffusion-controlled process in toluene.[49] This type of behavior is normally referred to as "static quenching", that is, diffusion is not required for quenching to occur, with the quencher already bound to the fluorophore before excitation takes place. In our system this requires 4aT to bind strongly to the AgFNP, in a similar fashion that 4aT binds to quantum dots.[4,46] Figure S6 shows fluorescence lifetime measurements

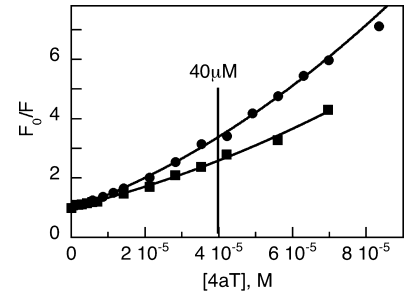

Figure 11. Stern−Volmer plot of fluorescence quenching of AgFNPs with 4aT in toluene. When analyzed using eq 2, the quenching rate constants obtained at low 4aT concentrations are above the diffusion-controlled rates, indicating a static quenching mechanism involving binding to the particle surface. The efficiency of quenching is significantly higher in the absence of cyclohexylamine (●) than in the presence of 40 μM cyclohexylamine (■) which implies a competition for surface sites between 4aT and cyclohexylamine.

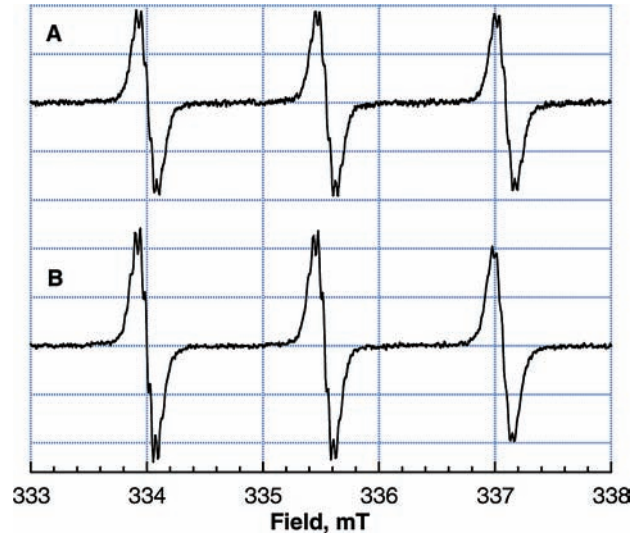

Figure 12. (A) EPR spectra of 18.0 μM 4aT in deaerated toluene; (B) deaerated toluene solution of concentrated AgFNPs ($A_{448} = 1.3$) and 18.0 μM 4aT. A decrease in the relative intensity of the high-field feature of 4aT in the presence of AgFNPs is observed. All EPR parameters for both spectra are included in the Experimental Section.

in the absence of 4aT and in the presence of 17 μM 4aT, corresponding to the F_0/F value of 2.1 in Figure 11. The fact that the fluorescence lifetime remains unchanged, while the maximum intensity decreases, is also indicative of a static quenching mechanism. The reasons for the upward curvature at moderately high 4aT concentrations are analyzed in the Discussion.

EPR Studies. EPR experiments were performed to observe if binding to the surface of the Ag particles was showing the same type of anisotropic line broadening observed in the case of 4aT bound to CdSe quantum dots.[47] As seen in Figure 12, there is no broadening of the low and midfield nitroxide peaks upon addition of concentrated Ag particle solution. However, there is a relative decrease in the peak-to-peak height of the high-field line, which was reproducible with many different batches of particles. Control experiments were performed by addition of synthetically prepared cyclohexylammonium trifluoroacetate, and no effects on the isotropic 4aT spectrum were observed. Therefore, we conclude that the small degree of anisotropy observed in Figure 12B is a result of 4aT binding to

(49) Turro, N. J.; Ramamurthy, V.; Scaiano, J. C. *Principles of Molecular Photochemistry: An Introduction*; University Science Publishers: New York, 2008.
(50) Turro, N. J. *Modern Molecular Photochemistry*; Benjamin/Cummings Publishing Co.: Menlo Park, 1978.
(51) Billone, P. S.; Maretti, L.; Maurel, V.; Scaiano, J. C. *J. Am. Chem. Soc.* **2007**, *129*, 14150–14151.
(52) Jin, W. J.; Fernandez-Arguelles, M. T.; Costa-Fernandez, J. M.; Pereiro, R.; Sanz-Medel, A. *Chem. Commun.* **2005**, 883–885.

the surface of the Ag particles.[53,54] The absence of broadening on the two low-field features suggests that the local environment of the bound nitroxide is close to that of free nitroxide where its axial degrees of rotational freedom are not hindered by a closely packed ligand environment.[55]

Discussion

Numerous methods are available for the reliable synthesis of metal nanoparticles, including silver.[6,56] Most of these methods employ reductants such as borohydride and stabilize the particles in solution with a variety of coatings to avoid or minimize precipitation.[32,57] Some of these protected layers can have biological functions incorporated. Typically silver nanoparticles show a distinct plasmon band which in our past work has been between 390 and 420 nm.[8,33] We were initially surprised when the absorption band obtained was closer to 450 nm (see Figure 1). We now believe that this absorbance is not due to the silver plasmon band but rather to the presence of small silver clusters. Previous studies have identified absorbance bands at 385, 410, and 442 nm, depending on their local geometries, as belonging to Ag dimers in Ar matrixes,[22] the latter which corresponds well to the absorption we observe in the present case at around 450 nm. As evident from the TEM images (Figure 9) and the observed weak absorption band at 390 nm in certain samples, large (3.4 nm) particles are formed in the photoreaction. We have been unable to determine the chemical yield of the small silver clusters versus the yield of larger nanoparticles. While the spectroscopic data for the particles are well documented[58] (and gives about 0.5 nM particles), that for the clusters is not; further, it is unclear if surface enhancement effects may influence the cluster optical properties. Gel permeation chromatography (GPC) was used in an attempt to verify that the fluorescence of the samples was associated with species attached to the larger nanoparticles but the fluorescence was unstable under these conditions, possibly due to on-column interactions.

In our case we have selected a photochemical reaction in order to generate the reducing species required, as shown in Scheme 1. While photochemical methods have been used before, the choice of chromophore and wavelength are frequently not optimized; the rationale for making suitable choices was discussed in a recent contribution.[35] Our approach has been to generate well-established reductive species, such as ketyl radicals, under conditions where the precursor (I-2959 in our case)[34,35] has strong absorptions, and where radicals are produced in fast processes that minimize or preclude quenching events. For example, although Ag^+ is an excellent excited-state quencher,[33,38] it is unable to quench significantly the triplet state of I-2959, which has a lifetime of just a few nanoseconds.[36]

Our transmission electron microscopy measurements reveal particles of about 3.4 mm in diameter, somewhat more polydisperse when they are prepared directly in toluene, compared with those synthesized in THF and then transferred into toluene. As a functional material, the description as 3.4 nm fluorescent silver nanoparticles is accurate but somewhat misleading. Metal nanoparticles of this size are not expected to fluoresce, and plasmon absorptions do not have a corresponding emission band. We believe that the emissions are due to small silver clusters, predominantly Ag_2 supported by the readily detectable nanoparticles and stabilized by the presence of protonated amines and trifluoroacetate anions. Further support for the presence of small fluorescent clusters comes from the remarkably clean monoexponential decay of the fluorescence, resembling that of simple molecules and a characteristic that is not usually observed with fluorescent nanoparticles, such as quantum dots, where fluorescence decay follows complex decay patterns. Other researchers have detected fluorescence in the 2−3 ns range and attributed it to Ag_2 clusters.[13,17,59] We have verified that any Ag^+ complexes that may form with either the starting reagents or any of the photoproducts are nonfluorescent, precluding the possibility of silver complexes contributing to the observed emission. We have also observed that the organic photoproducts themselves, which have been isolated, are not fluorescent either.

Small clusters are known to have a tendency for agglomeration. These aggregates of clusters still retain the key emissive properties of the individual clusters, although not surprisingly the solution behaviors lack the sharp excitation and emission profiles[17] that characterize small clusters in matrixes at cryogenic temperatures. The fact that these clusters, most likely Ag_2, survive on the nanoparticle surface may reflect the intrinsic bond strength of 160 kJ/mol in diatomic silver and further stabilization due to the amine and trifluoroacetate moieties.

A few studies have also noted that an excess of positive charges tends to facilitate particle or cluster stabilization.[18,39,60] In our case NMR provides unequivocal evidence that trifluoracetate ions are part of the surface coverage and perhaps a few ions are needed to neutralize excess Ag^+ charges. However, ammonium ions derived from the amine are clearly also on the surface. Most likely it is these hydrophobic groups (e.g., from hexadecylamine) that ultimately provide the compatibility with a very nonpolar solvent such as toluene. Small amines appear to fail to provide equivalent stabilization.

Once the particles have been purified and the excess salt (such as cyclohexylammonium trifluoroacetate) separated, the material retains some affinity for free amines. In the case of nitroxide free radicals, for instance, we see much higher quenching efficiency with 4aT than with TEMPO, which lacks the primary amine functionality. The quenching by 4aT is remarkably efficient, even when compared with the quenching of quantum dot emission by the same quencher.[4,47] These results can only be explained by invoking static quenching in which 4aT is strongly bound to the AgFNP surfaces, which appears to provide excellent access to the fluorescent clusters these particles support. The upward curvature (Figure 11), while small, is rather intriguing. In the case of quantum dots, quenching slots by 4aT leads to negative (downward) curvature, attributed to the replacement of TOPO (trioctylphosphine oxide) at high concentration, while in the low concentration regime, 4aT binds to available sites.[4,47,51] Using a similar rationale for AgFNP, one would conclude that the more difficult sites to access (i.e., at higher concentrations) are also the ones in closest proximity to

(53) Wertz, J. E.; Bolton, J. R. *Electron Spin Resonance. Elementary Theory and Practical Applications*; McGraw-Hill: Toronto, 1972.
(54) Weil, J. A.; Bolton, J. R. *Electron Paramagnetic Resonance: Elementary Theory and Practical Applications*, 2nd ed.; Wiley-Interscience: Hoboken, NJ, 2007.
(55) Chechik, V.; Wellsted, H. J.; Korte, A.; Gilbert, B. C.; Caldararu, H.; Ionita, P.; Caragheorgheopol, A. *Faraday Disc.* **2004**, *125*, 279–291.
(56) Eustis, S.; El-Sayed, M. A. *Chem. Soc. Rev.* **2006**, *35*, 209–217.
(57) Mirkhalaf, F.; Paprotny, J.; Schiffrin, D. J. *J. Am. Chem. Soc.* **2006**, *128*, 7400–7401.
(58) Link, S.; Wang, Z. L.; El-Sayed, M. A. *J. Phys. Chem. B* **1999**, *103*, 3529–3533.
(59) Fedrigo, S.; Harbich, W.; Duttet, J. *J. Chem. Phys.* **1991**, *99a*, 5712.
(60) Messere, A. G., A.; Garella, I.; Temussi, F.; Di Blasio, B.; Fiorentino, A. *Synth. Commun.* **2004**, *34*, 3317–3324.

the emissive clusters supported by the nanoparticles, thus leading to more efficient quenching (upward curvature). In any event the effect is small and quenching remarkably effective, even more so when the short excited state lifetime (~2.6 ns) is taken into account.

One may ask if small silver clusters, specially Ag_2, are free in solution or associated with AgNP such as imaged by TEM and shown in Figure 9; as already indicated, we favor the latter explanation. The data in Figures 10 and 11 provide support for this interpretation. Quenching data support that 4aT binds strongly to the luminescent species (i.e., quenches efficiently), and earlier work shows strong binding to nanoparticles.[4,8,47,48,61] Thus, when we add 40 μM cyclohexylamine, as it binds to the nanoparticle surface we would expect more 4aT to become available in the solution and less at the particle surface. Thus, if the emissive Ag_2 was located in the solution, addition of cyclohexylamine would lead to enhanced quenching by 4aT, since displacement of 4aT from the nanoparticle surface would make more available for quenching in the solution. In contrast, we observe reduced quenching, consistent with the fact that cyclohexylamine displacement of 4aT from the surface also reduces abundance of quenchers in the proximity of the fluorescent clusters. Further, it would be hard to see how Ag_2 free in solution could lead to curved Stern−Volmer plots, since Ag_2 should show molecular-type quenching behavior.

Fluorescence microscopy images in polystyrene films (a polymer structurally similar to the toluene solvent used here) demonstrate unequivocally that the emission arises from discrete particles, thus also supporting the conclusion that the emissive clusters are located at or near the AgNP surface. One such image is shown in Figure 10.

In the past few years a number of contributions have reported on the bright emission from small silver clusters;[11] their properties are such that aqueous systems are interesting from a biological perspective and have already been examined in DNA and in cells.[13,27,29,62,63] On the other hand, AgFNP soluble in nonpolar organic media may have applications in polymeric functional materials; further, photochemical synthesis provides a route for imaging and the efficient fluorescence a mechanism for mapping material distribution. These nanoparticle-supported clusters may also have interesting catalytic properties.

In conclusion, we recently pointed out that ketones are good sensitizers for nanoparticle synthesis not because of the energy they can deliver but rather because of the free radicals they can generate.[35] The synthesis and characterization of AgFNP shows the generality of these concepts and the fact that ketyl radicals are excellent tools for nanoparticle synthesis. In the example reported here, nanoparticles synthesized are around 3 nm in diameter but their fluorescent properties are derived from small silver clusters, predominantly Ag_2, that are believed to be located at the nanoparticle surface or stabilization layer. It is possible that interaction with the surface contribute to the high emission quantum yield observed (0.11−0.15). The new AgNFP are interesting functional materials with potential applications in imaging and nanophotonics. Their excellent long-term stability and excellent solubility in organic solvents may prove key to future applications.

Acknowledgment. We acknowledge financial support from the Natural Sciences and Engineering Research Council of Canada (NSERC), CFI, and the Government of Ontario. Thanks are due to Professor Gonzalo Cosa and Mr. Pierre Karam (McGill University) for their help in acquiring the spectrum in Figure S10.

Supporting Information Available: Absorption spectra, comparison of excitation and emission spectra in THF and in toluene, spectral data used to obtain fluorescence quantum yields, the fluorescence lifetime in the presence of 4aT, ^{19}F and H NMR data, the histogram of particle size distribution and Stern−Volmer plot of fluorescence quenching by TEMPO. This material is available free of charge via the Internet at http://pubs.acs.org.

JA900201K

(61) Thomas, K. G.; Kamat, P. V. *J. Am. Chem. Soc.* **2000**, *122*, 2655–2656.
(62) Ritchie, C. M.; Johnsen, K. R.; Kiser, J. R.; Antoku, Y.; Dickson, R. M.; Petty, J. T. *J. Phys. Chem. C* **2007**, *111*, 175–181.
(63) Richards, C. I.; Choi, S.; Hsiang, J. C.; Antoku, Y.; Vosch, T.; Bongiorno, A.; Tzeng, Y. L.; Dickson, R. M. *J. Am. Chem. Soc.* **2008**, *130*, 5038.